Multifunctional stratified composite coatings by electrophoretic deposition and RF co-sputtering for orthopaedic implants

J Mater Sci (2021) 56:7920–7935

Composites & nanocomposites

Multifunctional stratified composite coatings by electrophoretic deposition and RF co-sputtering for orthopaedic implants

Qaisar Nawaz[1], Steffen Fastner[1], Muhammad Atiq Ur Rehman[2], Sara Ferraris[3], Sergio Perero[3], G. Gautier di Confiengo[4], Emre Yavuz[5], Monica Ferraris[3], and Aldo R. Boccaccini[1,*]

[1] *Institute of Biomaterials, Department of Material Science and Engineering, University of Erlangen-Nuremberg, Cauerstr.6, 91058 Erlangen, Germany*
[2] *Department of Materials Science and Engineering, Institute of Space Technology Islamabad, Islamabad 44000, Pakistan*
[3] *Institute of Materials Physics and Engineering, Department of Applied Science and Technology, Politecnico Di Torino, 10129 Torino, Italy*
[4] *Institute of Science and Technology for Sustainable Energy and Mobility (STEMS), Strada delle Cacce 73, 10135 Turin, Italy*
[5] *Institute of Science, Department of Chemistry, University of Akdeniz University, 07058 Antalya, Turkey*

Received: 18 October 2020
Accepted: 21 December 2020
Published online: 2 February 2021

ABSTRACT

In this study, multifunctional stratified antibacterial and bioactive coatings were deposited and characterised. Initially, PEEK/bioactive glass (BG)/ mesoporous bioactive glass nanoparticle (MBGN) layers with a thickness of 110–120 µm were deposited on stainless steel substrates using electrophoretic deposition (EPD). Thin silver nanocluster-silica composite layers with a thickness of 70–155 nm were then deposited by radio frequency (RF) co-sputtering on the previously deposited EPD coatings. The deposition was carried for two different sputtering times (20 min and 40 min), which led to different layer thicknesses. PEEK/BG/MBGNs coatings were also deposited via single-step EPD. A comparison between the physicomechanical and biological characteristics of single layer PEEK/BG/MBGNs composite coating and bilayer Ag-PEEK/BG/MBGNs is presented. Scanning electron microscopy (SEM) and energy-dispersive x-ray spectroscopy (EDX) indicated that silver nanoclusters were homogeneously distributed in the multilayered EPD/RF coatings. An apatite-like structure was formed on the surface of the coatings upon immersion in simulated body fluid (SBF) after 1 day. Silver nanoclusters embedded in the silica matrix as a top layer provided controlled release of silver ions which led to a potent antibacterial effect against *E. coli* and *S. carnosus*. Single layer coatings exhibited a burst

Handling Editor: Catalin Croitoru.

Address correspondence to E-mail: aldo.boccaccini@ww.uni-erlangen.de

https://doi.org/10.1007/s10853-020-05725-w

release of Ag ions, which led to antibacterial effects but were toxic to osteoblast cells. Finally, the results of WST-8 assays confirmed that the multi-structured coatings allow osteoblast-like cells to proliferate and attach strongly on the surface of the coatings.

Introduction

Orthopaedic implants are used to restore the structure and function of damaged or diseased parts of bones or joints with the aim of improving the life quality of individuals. Orthopaedic implants intended to be used under mechanical loads should have favourable mechanical strength and long-term stability [1–3]. Metallic implants usually have favourable mechanical properties, for example Co–Cr alloys, stainless steel, titanium and its alloys are normally used in orthopaedic implants [4, 5]. Although they are mechanically resilient, dissolution of metal ions from them into the body may cause inflammation around the metal implant [2]. Therefore, surface modification of metallic implants should be considered, which should improve the interfacial contact of metallic implants with surrounding tissues. In a common approach, the implants are coated with bioactive materials [5]. Common bioactive materials considered to coat metal surfaces are bioactive ceramics, such as hydroxyapatite and bioactive glasses (BGs) [1, 3, 6, 7]. The applied (deposited) coatings on implants should provide various positive characteristics such as corrosion resistance, wear resistance, antibacterial properties, and they should support bone cell adhesion [8, 9].

Bioactive glass (BG), invented by Hench et al. [10, 11], facilitates the formation of a strong bond between implant and bone via the in-situ formation of a hydroxyapatite (HAp) layer similar to the mineral phase of bone. Bioactive glasses are prepared using melt quenching and sol-gel techniques [12]. Sol-gel derived glasses offer versatility in composition, size and morphology. The high surface area of sol-gel derived BGs favours the formation of an apatite layer thus leading to the effective contact between the implant and bone [13, 14]. BG can be further modified by incorporating several biologically active metallic ions such as Cu, Ag, Au, Sr and Mn [15–17]. The doping of BGs with Ag and Cu ions is a well-known approach for providing potent antibacterial effect against a wide spectrum of bacteria. Nevertheless, the uncontrolled release of silver and copper ions can be toxic for osteoblast cells, which negates the mentioned benefitial antibacterial effect making the materials non-suitable for biomedical applications [14, 15, 18].

Despite the fact that BGs can provide excellent bone binding properties, BGs cannot be used in load bearing applications due to their brittle nature. Therefore, BGs are often used in combination with various synthetic polymers such as polyether ether ketone (PEEK), polymethyl methacrylate or with natural polymers (chitosan, gelatin, etc.) [19–21]. The combination of PEEK and BG has been investigated by various researchers during the last decade for biomedical applications [20, 22–24]. PEEK can avoid stress shielding issues that may arise due to the high elastic modulus of metals in comparison to bone [19]. The combination of PEEK and BG can be tailored to achieve elastic modulus close to that of natural bone [20]. Furthermore, PEEK/BG coatings can act as a robust barrier between the bone and the metallic implant. PEEK/BG coatings have also shown cytocompatibility to osteoblast cells [24–26]. However, the successful incorporation of antibacterial agents into PEEK/BG composites remains a challenge. Seuss et al. [26] incorporated silver in PEEK/BG composites by electrophoretic deposition (EPD). These coatings show an antibacterial effect against Gram-positive and Gram-negative bacteria but the uncontrolled release of Ag ions represents a challenge. EPD is a simple room temperature coating technique which requires preparation of stable suspensions (of the particles/molecules which are intended to be deposited) followed by migration of the particles/molecules to the oppositely charged electrode upon the application of an electric field [21, 27].

Rehman et al. [28] employed a strategy based on multilayer coating structures consisting of PEEK/BG layers (deposited via EPD) coated with silver/silica nanoclusters (deposited by radio frequency (RF) co-sputtering). The developed multi-structured coatings

were bioactive and antibacterial. However, the release of Ag ions from such multi-structured coatings was not investigated. In addition, the cytotoxic effect of released silver ions should also be investigated.

Radio frequency (RF) magnetron sputtering as a coating technique provides multiple advantages including high efficiency, favourable coating-substrate bonding strength and controllable properties, as demonstrated for the fabrication of HAp bioactive coatings [29]. For example, Chernozem et al. [30] deposited CaP coatings via RF magnetron sputtering showing that the coatings improved the mechanical and biological properties of the substrate. In another study Surmenev et al. [31] showed that HA coatings can be deposited on polymeric substrates via RF magnetron sputtering, which anticipates that the technique is a suitable choice for depositing thin films on PEEK-based layers, as intended in the present study.

In this study, therefore, composite coatings based on PEEK, BG and Ag-MBGNs were developed via a single-step EPD process. Subsequently, RF co-sputtering of Ag silica nanoclusters on the previously obtained EPD coatings was employed at two different sputtering times, i.e. 20 min and 40 min.

Experimental procedure

Materials and suspension preparation

EPD of MBGN/BG/PEEK

Mesoporous bioactive glass nanoparticles (MBGNs) were synthesised by modifying the process discussed elsewhere [12]. The MBGNs were prepared in two nominal compositions, i.e. 70 SiO_2, 30 CaO (wt. %), and 70 SiO_2, 27 CaO, 3 Ag_2O (wt. %), named as MBGNNs and Ag-MBGNs, respectively. PEEK powder (average particle size of 10 µm, 704XF Victrex^{TM}) and 45S5 bioactive glass (BG) powder (4-µm average particle size, Schott, Germany) with nominal composition 45 SiO_2-24.5 Na_2O- 24.5 CaO-6 P_2O_5 (wt. %) were used.

Two types of suspensions were prepared in ethanol; one with PEEK, BG and MBGNs and the other with PEEK, BG and Ag-MBGN. The EPD suspensions were prepared by mixing MBGNs/Ag-MBGNs and BG powders (both 5 g L^{-1}) in ethanol under continuous stirring. The solution was stirred for 2 h followed by 15 min ultrasonication (ultrasonic bath Sonorex RK 100 by Bandelin electronic GmbH & Co. KG) and 15 min of magnetic stirring simultaneously in order to avoid the formation of agglomerated particles. Then, the PEEK powders (20 g L^{-1}) were added and the suspensions were stirred for 10 min.

316 L stainless steel (SS) foils (30 X 15 mm^2) were used as deposition substrates and counter electrodes, respectively. The coatings were deposited under an electric filed of 100 V/cm with 30 s of deposition time (these parameters were optimised using Design of Experiments approach in a previous study [20]). The sintering of the coatings was performed in a muffle furnace (Nabertherm^{TM} GmbH) at 400 °C for 30 min with a heating rate of 2 °C/min. The sintered coatings that consist of PEEK/BG/MBGNs layers (EPD layer) were further coated with a thin Ag-SiO_2 layer by using RF Co-sputtering.

RF co-sputtering of silver nanoclusters-silica composite

The composite top layer (Ag nanocluster embedded in a silica matrix) was deposited on the PEEK/BG/MBGNs substrates (deposited via EPD process, as described in the previous section) using the Radio frequency (RF) co-sputtering (Microcoat^{TM} MS450) process, as described in detail in reference [28]. These Ag/SiO_2 nanoclusters were deposited by applying 200 W in RF mode and 1 W in direct current to silica and silver targets, respectively. The Ag/SiO_2 ratio was tailored to avoid an excess of Ag (higher concentration of Ag may lead to toxicity). The Ag/SiO_2 ratio was adjusted by applying a duty cycle to the Ag target; the plasma on the Ag target was turned-on for 1 s after every 24 s through the whole deposition process of 20 and 40 min [32]. Pure Argon atmosphere was used with a deposition pressure of 5.5 dPa, and the pressure before deposition was below 0.01 mPa. Two different sputtering times were considered, i.e. 20 min and 40 min, according to the previous results [33, 34]. These coatings were labelled as EPD/RF-20 and EPD/RF-40, respectively. The higher sputtering time led to higher thickness and amount of silver in the coatings, as discussed in our previous study [28]. The experimental set-up by which multi-structured composite coatings were obtained is shown in Fig. 1.

Characterisations of the coatings

Topographical, morphological and mechanical investigations

The surface topography and cross-section of coatings were examined using scanning electron microscopy (SEM) (LEO 435VP, Carl Zeiss™ AG). Prior to this, the coatings were coated (Q150/ S, Quorum Technologies™) with gold. The presence of elements in the coatings was qualitatively detected using energy-dispersive x-ray spectroscopy (LEO 435VP, Carl Zeiss™ AG). Crystalline structure of the coatings was investigated by x-ray diffraction (XRD) analysis (MiniFlex 600, Rigaku Corporation, Europe) with Cu Kα radiation (λ = 0.154 nm) using the 2θ range of 20°–80° with a step size of 0.02° and dwell time of 2° per minute.

The adhesion and scratch resistance of the coatings was assessed via scratch tests (CSM™ Revetest machine). A load of (1 – 50) N was applied on the surface through a Rockwell C diamond indenter (200 μm). The indenter speed of 5.2 mm/min and a loading rate of 50.96 N/min were used. The critical load corresponding to coating detachment (Lc1) was estimated based on optical images and acoustic emission (AE) results. The techniques allow a semi-quantitative assessment of the coating adhesion and scratch resistance. The obtained values are not intended to be considered as absolute values but as indication of the range of adhesion/scratch resistance and are useful for the comparison and ranking of different materials.

In vitro bioactivity assessment

The bioactivity of coatings was determined by immersing samples in simulated body fluid (SBF), as proposed by Kokubo et al. [35]. The selected coatings were immersed in SBF and placed in an orbital shaker fixed at 37 °C for predetermined time points. After each time point, samples were removed from SBF and dried at 60 °C. The formation of

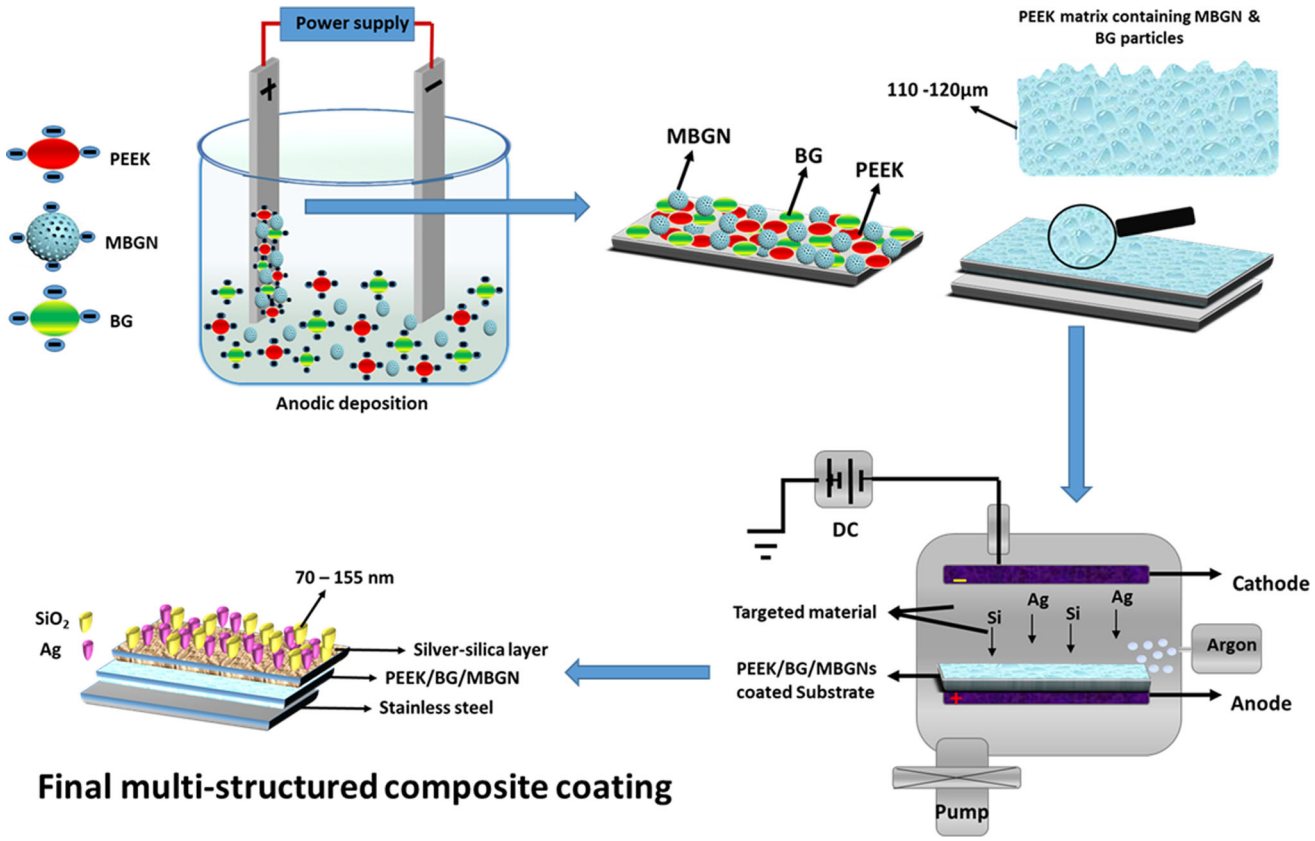

Figure 1 Experimental set-up to obtain multi-structured coatings via EPD and RF co-sputtering.

hydroxyapatite (HAp) crystals on the surface of coatings was examined using FE-SEM, EDX and XRD.

Ion release in PBS

The silver ion release profiles of coatings were monitored in phosphate-buffered saline (PBS) at 37 °C in the dark. Briefly, each coating was immersed in 6 ml of PBS for 7 days, and every day 5 ml solution replaced with 5 ml fresh PBS. The collected solutions at different times were analysed by using atomic absorption spectrophotometer (AAS, Shimadzu, AA-7000) to obtain cumulative silver ion release profiles of the coatings. Each test was performed in triplicate, and mean values were reported.

In vitro cytotoxicity and cell attachment

All coatings were disinfected by exposing them to UV light. In-vitro cytocompatibility of coatings towards MG-63 osteoblast-like cell line (Sigma-Aldrich) was evaluated using water-soluble tetrazolium (WST) assay. Cell culture medium was prepared using Dulbecco's modified Eagle's medium (DMEM; Gibco) supplemented with 10 vol. % fetal bovine serum (FBS; Sigma-Aldrich) and 1 vol. % penicillin/streptomycin (Pen-Strep; Sigma-Aldrich). MG-63 cells were cultured in cell culture medium and incubated at 37 °C for 48 h at 5% CO_2 to achieve ~ 80–90% confluency. The effect of silver release towards MG-63 cells was tested via direct (cells seeded on the top surface of the coatings) and indirect approaches (cells exposed to extracts of coatings).

Indirect approach

In the indirect approach, the sterilised samples were soaked for 24 h in 1 mL of DMEM medium. After 24 h, the extracts of the coatings containing silver ions were collected. Different volume of aliquots (100, 200, 300, 500,750 and 1000 µL) were poured into a 24 well plate, where cells were already seeded (10^5 cells/per well) for further cell studies. The total volume of all wells was maintained at 1 ml, which contains aliquots of coatings, seeded cells and DMEM medium. The cells were then allowed to grow for 2 days at 5% CO_2 and 37 °C. The cell viability was measured using the WST-8 test (Sigma-Aldrich), and the optical density (OD) at 450 nm was measured as described above. The cell proliferation was quantified against the calibration curve.

Direct approach

In the direct approach, the pretreated samples were placed in 24-well plates, in which 200 µL of cell suspension (10^5 cells) were seeded and incubated at 37 °C with 5% CO_2. Afterwards, 800 µL of cell culture medium was added to the well plate for further cell culturing. The cells were then allowed to grow for 2 days. The cell viability was quantified by the WST-8 test (Sigma-Aldrich), as described elsewhere [16]. The 100 µL of supernatant was taken from all coatings and the optical density (OD) at 450 nm was measured with a spectrophotometer (Synergy HT Multidetection Microplate, USA). The cell viability was quantified according to the following formula:

$$Cell\ viability = \frac{OD(sample) - OD(blank)}{OD(reference) - OD(blank)} x100\%$$

The cells present on the surface of coatings were fixed using a fixing solution. The fixing solution was prepared by mixing 3 vol% of paraformaldehyde and glutaraldehyde (Sigma-Aldrich, Germany) in 0.2 M sodium cacodylate (Sigma-Aldrich, Germany) buffer solution. Afterwards, the coatings were washed with ethanol and dried via critical point dryer (Samdri PVT-3; Tousimis Research Corp., USA). After drying, cell morphology was examined by SEM.

Antibacterial study

An antibacterial test was conducted to investigate the effect of released silver. This was done by performing agar disks diffusion test on selected coatings. Before this, the coatings were sterilised under UV light. The 20 µl of LB-media containing Gram-negative (*Escherichia coli*) and Gram-positive (*Staphylococcus carnosus*) bacteria were spread homogeneously on the agar plate. Coatings were gently put on the agar plates and incubated at 37 °C for 24 h. After this, digital images were taken, and the zones of inhibition were measured via 'ImageJ'. All the experiments were done in triplicate.

Results and discussion

Microstructural analysis of Ag-EPD composite coatings

Figure 2 shows SEM images of the as-synthesised mesoporous bioactive glass nanoparticles (MBGNs) (Fig. 2a) and of a composite coating deposited by EPD at an applied electric field of 100 V/cm for 30 s (Fig. 2b). A cross-sectional image of produced EPD (PEEK/BG/MBGNs) coating is shown in Fig. 2c. The composite coating consists of BG microparticles and MBGNs embedded in the PEEK matrix. The mesoporous bioactive glass nanoparticles are uniform, homogeneous and have spherical morphology with average particle size of 120 ± 10 nm (calculated using image J, data not shown here), as shown in Fig. 2a. Figure 2b shows that the MBGNs and BG particles are dispersed uniformly in the PEEK matrix. It was observed that the coating contains some micropores (Fig. 2b), which will allow the top layer to infiltrate into the underlaying layer. The cross-sectional image of the Ag-EPD coating is shown in Fig. 2, which has a coating thickness of $\sim$ 110 µm (Fig. 2c). The cross-section of the sample was prepared by wire cutting, which cause the delamination of coatings (Fig. 2c). A similar range of coating thickness has been reported for PEEK-based composites in the literature, and similar coatings based on PEEK/BG were deposited on 316L SS via EPD [20, 22, 23, 36]. The resultant coatings showed a similar microstructure and thickness as those of PEEK/BG coatings (Fig. 2b).

Sputtering condition 1 (EPD/RF-20)

RF co-sputtering was used to deposit a thin Ag-SiO_2 composite layer on EPD coatings. The multi-structured coatings obtained via RF sputtering and EPD were compared with Ag-EPD coatings to ascertain the loaded value of the Ag–SiO_2 RF layer. It has been reported that a homogeneous layer of Ag–SiO_2 nanoclusters can be deposited by RF co-sputtering techniques [32, 33, 37–39].

The unrestrained release of silver ions can be cytotoxic [28]. However, in the presence of a thin Ag–SiO_2 layer, in which silver nanoclusters are embedded, the silica matrix restrains the excessive release of silver ions [39]. The morphology of the Ag–SiO_2 composite thin layer, which is deposited on the top of an EPD PEEK/BG layer for 20 min (EPD/RF-20), is shown in Fig. 3. Moreover the thin Ag-SiO_2 layer ($\cong$ 60 nm) was deposited on the PEEK/BG/MBGNs coating. Despite the presence of the top layer, the morphology of the PEEK/BG/MBGNs (bottom) layer was still visible, as shown in Fig. 3a. Contact surface profiler (not shown here) was used to measure the thickness of the RF-sputtered silver-silica layer. The silver nanoclusters are only visible at higher magnification (Fig. 3b).

The amount of silver embedded in the top layer was lower than the detection limit of EDX (data now shown here). However, the RF sputtering of silver-silica nanocluster at the same parameters with 15 min of sputtering time, yields atomic ratio of 0.37 ± 0.015 for (Ag/(Ag + Si)) [32]. However, in the current work, the composition of silver in the top layer could not be measured because of the complex

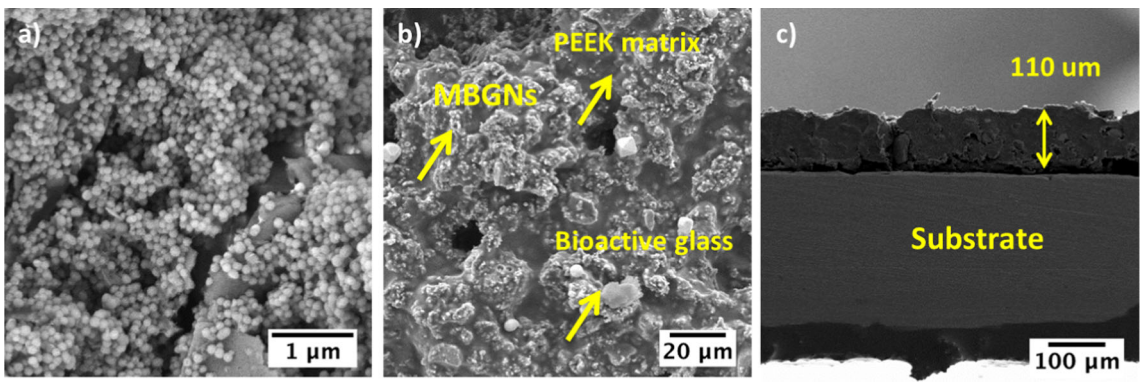

Figure 2 **a** As-synthesised mesoporous bioactive glass nanoparticles (MBGNs), **b** EPD composite coatings that were deposited at an applied electric field of 100 V/cm for 30 s and **c** cross-sectional image of produced EPD (PEEK/BG/MBGNs) coating.

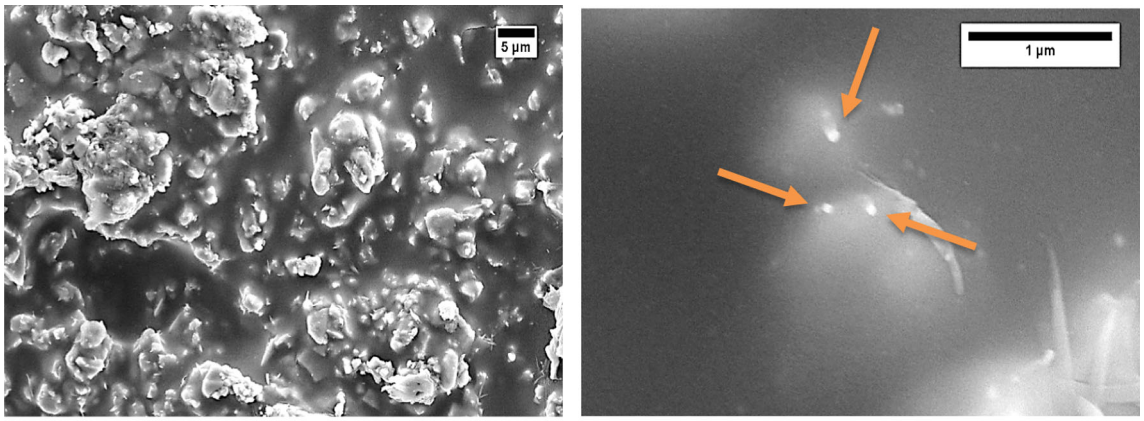

Figure 3 The morphology of silver nanocluster-silica composite layer deposited via RF co-sputtering on PEEK-BG (EPD) layer for 20 min (EPD/RF-20); **a** at low magnification and **b** at higher magnifications, in which small silver nanoclusters embedded in silica matrix are slightly visible (arrows).

multilayer composite coating's structure and high roughness of the bottom EPD layer.

Sputtering condition 2 (EPD/RF-40)

The morphology of Ag nanocluster-SiO_2 coatings deposited via RF co-sputtering with deposition time of 40 min when 200 W RF and 1 W dc were applied to silica and silver targets, respectively, is shown in Fig. 4. Figure 4 shows the typical cauliflower-like morphology of silver nanoclusters-silica layers [40]. Silicon wafer was used as a model sample to deposit coatings using the same parameters, which were further used to determine coating thickness. The thickness of the deposited silver-silica nanocluster thin layer on model samples was measured using contact surface profilometer [40]. It was found that coatings of thickness ≅ 100 nm were deposited, which were homogeneous and reproducible on the different substrates. The EDX spectrum (Supplementary figure S1) contains peaks associated with Si, Na, Ca and P and Ag, which are the constituents of BG and MBGNs. It was observed that the intensity of the silica peak increased (qualitatively) in the EPD/RF-40 sample (represented as red line in supplementary figure S1) compared to that of the EPD layer (represented as yellow line in supplementary figure S1), which indicates the presence of a silica matrix deposited by RF co-sputtering. Moreover, the presence of an Ag peak in the EPD/RF-40 sample confirmed the presence of Ag nanoclusters embedded in the silica matrix.

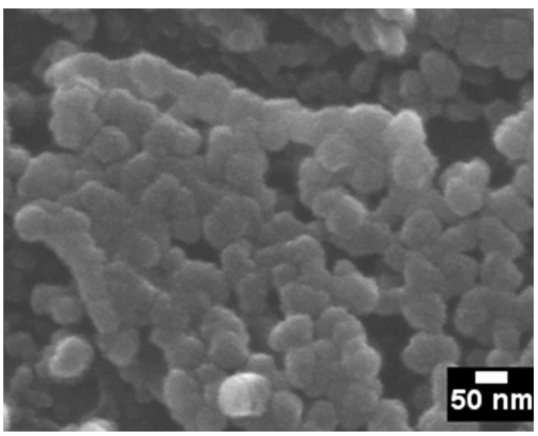

Figure 4 SEM micrographs of silver nanocluster-silica composite deposited on the EPD layer via RF co-sputtering for 40 min (EPD/RF-40).

Adhesion strength/scratch test

The adhesion and scratch resistance of deposited Ag-EPD, EPD/RF-20 and EPD/RF-40 coatings was assessed via the scratch test, as illustrated in Fig. 5. Due to the inhomogeneity of the coatings (high roughness), it is difficult to precisely individuate the critical loads at which the coating detaches. However, some interesting consideration can be made based on the scratch test coupled with acoustic emission results. The evaluation is semi-quantitative but allows a significant comparison between the tested materials. In EPD/RF-20 and EPD/RF-40 coatings the first critical load has been identified as the load at which the track becomes visible, and a small damage

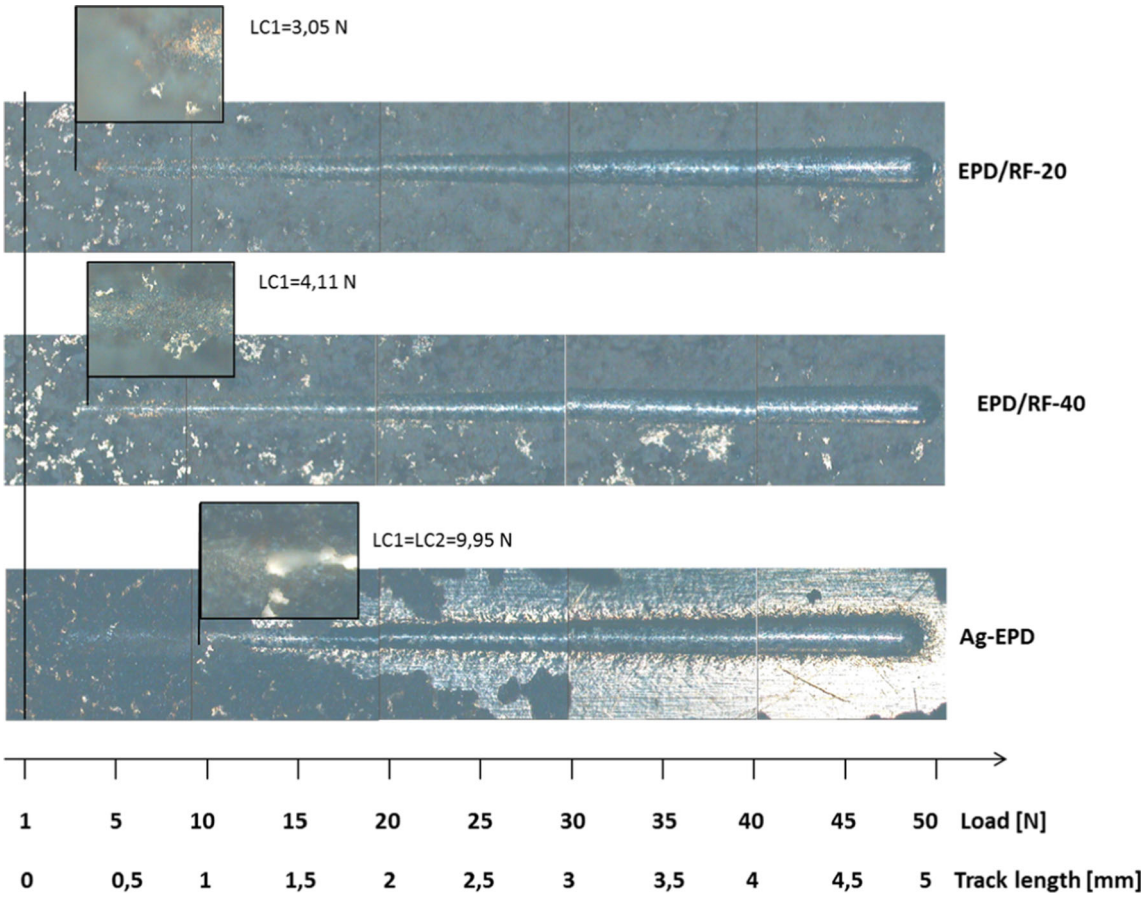

Figure 5 Results of the scratch test for Ag-EPD, EPD/RF-20 and EPD/RF-40 coatings.

to the coating (appearance of shiny spots attributable to the metallic substrate) can be evidenced. This load is similar for the two coatings, and it was estimated to be between 3 and 4 N (Fig. 5). From this point on a moderate increase in the damage at the centre of the track can be observed but there was no evidence of the presence of cracks or complete coating detachment up to 50 N (track end). A different behaviour can be observed for EPD samples. In this case the first damage is almost coincident with the coating complete detachment, which is close to 10 N. These results suggest that the SiO_2–Ag sputtered coating can confer a certain mechanical protection which can prevent its complete detachment even at high scratch loads. Furthermore, Rehman et al. [28] used a similar approach to obtain multifunctional coatings by the combination of EPD and RF co-sputtering, which was done at two different sputtering conditions. However, the adhesion strength in their coatings [28] was lower in comparison to the values determined in the present study. This confirms that the nanosized BG particles used in the present coatings, acting as fillers in the PEEK matrix, improve the adhesion strength.

A confirmation of the different detachment behaviour is provided by analysing the acoustic emission signal intensities generated by scratching (Fig. 6). The acoustic emission (AE) corresponds to the beginning of propagation of cracks during the scratch test. No difference was found in the AE results, as in the case of the critical load values (Lc1), between EPD/RF-20 and EPD/RF-40 coatings. Only AE results for EPD/RF-20 and Ag-EPD were reported. As shown in the graph (Fig. 5), the AE intensity of the EPD/RF-20 sample started 0.40 mm from the beginning of the scratch track, equivalent to 3 N (Lc1). With regards to the Ag-EPD samples, the AE increase was recorded 0.9 mm from the beginning of the scratch track, which corresponds to almost 10 N. A different behaviour between the two samples was observed also in the AE intensity: EPD/RF-20 reached a maximum intensity of 60% while Ag-EPD reached almost

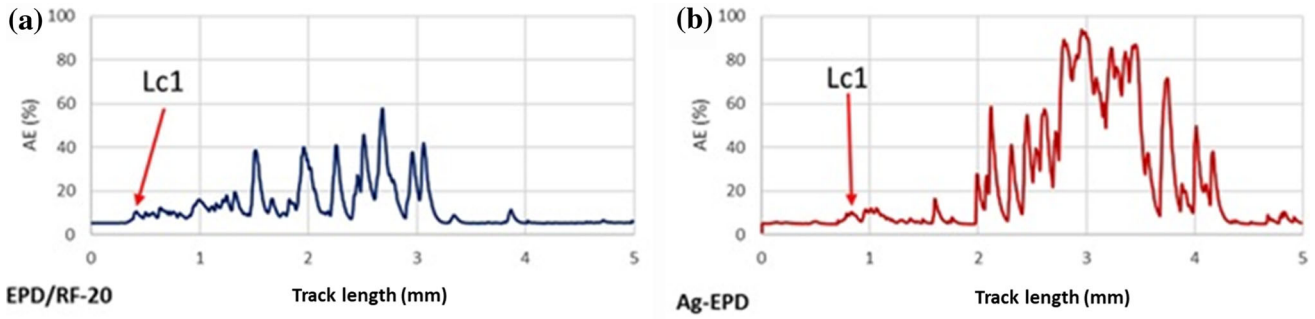

Figure 6 Acoustic emission (AE %)-track length (mm) curves generated during scratch test of (**a**) EPD/RF-20 and (**b**) Ag-EPD samples.

the full intensity (93%). The highest AE value of Ag-EPD coatings could be due to the continuous coating detachment as evident from Fig. 5.

In vitro bioactivity assessment

EPD/RF-40 coatings formed hydroxyapatite on their surfaces after 1 day of immersion in SBF, as indicated in Fig. 7. Figure 7a, b shows the change in the morphology of the coatings compared to the sample before immersion in SBF. A "cauliflower-like" morphology was observed, which indicated the formation of hydroxyapatite crystals on the surface of the EPD/RF-40 coatings (Fig. 7a). Higher magnification images (Fig. 7b) showed that the structure formed on the surface of EPD/RF-40 samples appears to be plate-like. Figure 7c shows that after 14 days of incubation deposits with "cauliflower like" morphology spread over the surface of the EPD/RF-40 coatings. Higher magnification images revealed that the plate-like structure was denser compared to that of the microstructure seen (Fig. 7b) after 1 day of

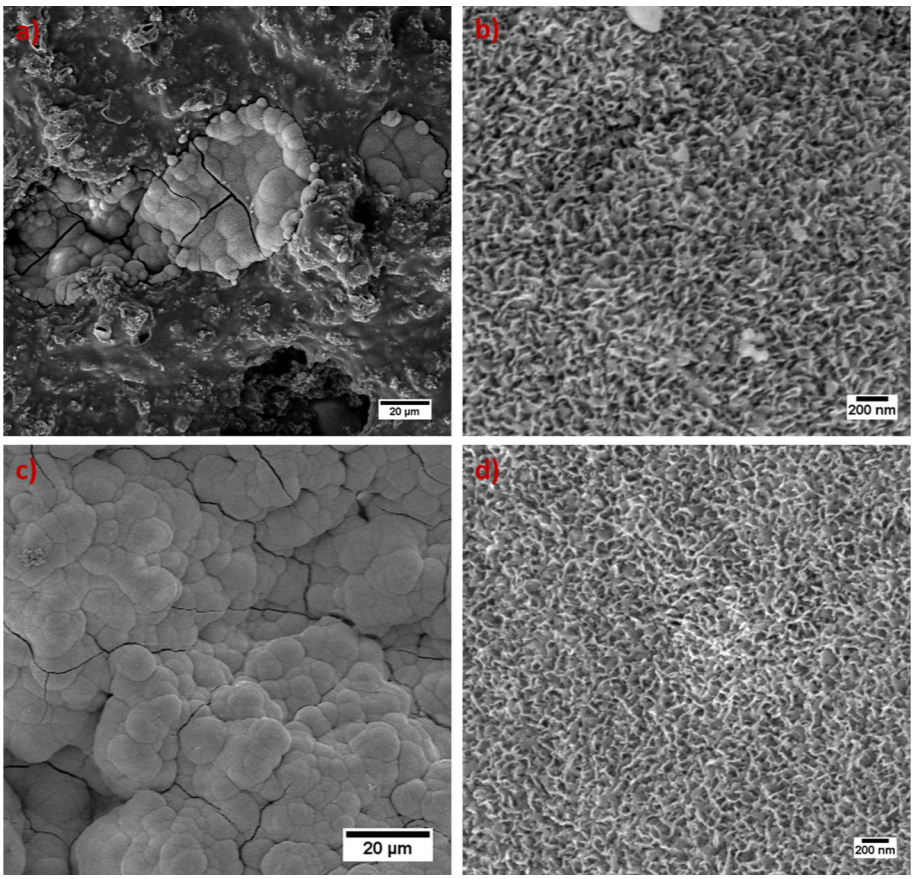

Figure 7 SEM images and EDX analysis of the EPD/RF-40 coatings after immersion in SBF for (**a**) 1 day, (**b**) 1 day at high magnification, (**c**)14 days, (**d**) 14 days at high magnification.

incubation [41]. Moreover, after immersion of coatings in SBF, an increase in intensity of Ca and P peaks and a decrease in the intensity of the Si peak was observed (Supplementary figure S2). This increase in intensity of Ca and P peaks indicated the formation of a calcium phosphate phase on the surface of the coatings [8, 28, 42]. These SBF immersed coatings were further characterised using XRD, which revealed the presence of crystalline peaks around 2θ = 25° and 33°. These peaks can be ascribed to the formation of an apatite-like phosphate phase (JCPDS 09–0432), as shown in Fig. 8 [43, 44]. In addition, the relative intensity of these crystalline peaks increases with increased SBF immersion time (Fig. 8), which is a typical characteristic of bioactive coatings (qualitatively) [41, 44]. Overall, all coatings showed bioactivity and the top RF-sputtered layer had no negative effect on bioactivity.

The in-vitro bioactivity of the Ag-EPD and EPD/RF-20 samples was not investigated in this work. In fact, the in vitro bioactivity of PEEK/BG coatings is well established and has been reported in our previous studies [24, 28, 45]. Here, we conducted in vitro bioactivity studies only on EPD/RF-40 samples in order to confirm that the top layer does not affect the bioactive character of the underlying PEEK/BG/MBGNs layer. Since EPD/RF-40 samples (coatings with higher Ag content) were bioactive, it was anticipated that coatings with lower silver content (EPD/RF-20) would not negatively affect the bioactivity of the PEEK/BG/MBGNs layer.

Silver ion release assessment

The ion release results in PBS showed that the release of silver ions from Ag-EPD coatings was three times higher compared to that from EPD/RF coatings (Fig. 9). A slow and sustained silver ion release was observed for EPD/RF-40 and EPD/RF-20 coatings. The high release of silver ions from Ag-EPD coatings can be due to the presence of silver doped mesoporous bioactive glass nanoparticles (Ag-MBGNs) on the surface of Ag-EPD coatings. In contrast to this, multi-structured coatings (EPD/RF-40 and EPD/RF-20) showed reduced release rate of silver ions which may be due the fact that the silica matrix (top layer) provides a barrier for Ag ions. Moreover, the presence of a high average roughness of the underlying (EPD) layer facilitates that the top layer (Ag nanocluster-silica layer) infiltrates the EPD layer, which can contribute to the slow release of Ag ions. Similar results for the release of the drug Lawson were achieved by Ur Rehman et al. from similar coatings [8, 25], who reported the controlled release of the drug due to the infiltration of the top layer in the cavities of the underlying coating. As expected, multi-structured coatings (EPD/RF-coatings) showed controlled release of silver ions, that can be beneficial for designing bioactive, antibacterial and cyto-compatible coatings for orthopaedic applications.

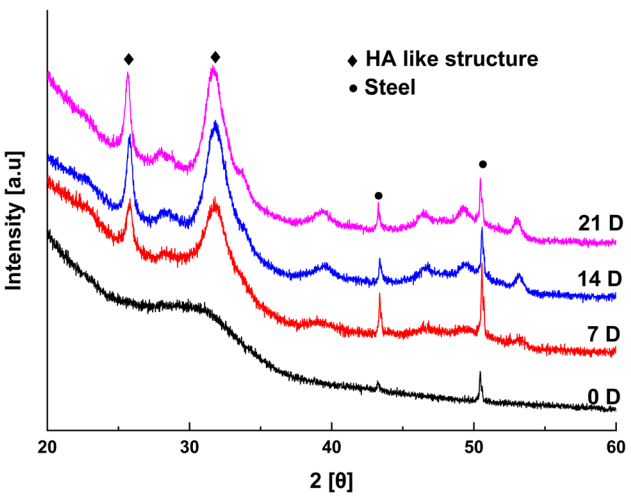

Figure 8 XRD analysis of EPD/RF-40 coatings before and after immersion in SBF.

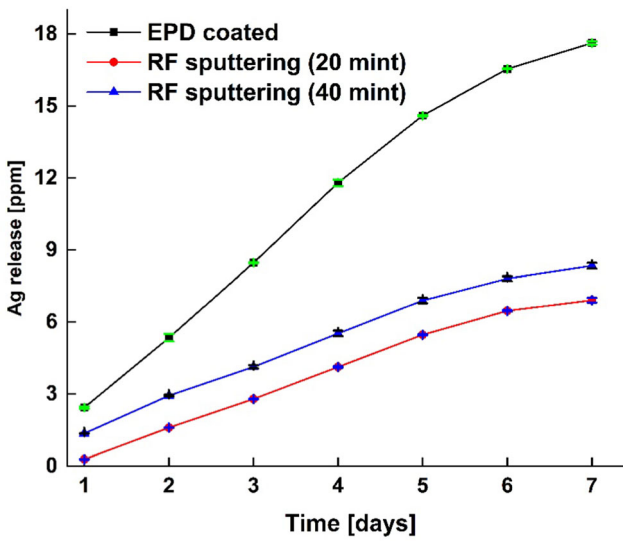

Figure 9 Silver ion release of Ag-EPD, EPD/RF-20 and EPD/RF-40 coatings in PBS.

In vitro cell studies

The cell compatibility of Ag-EPD, EPD/RF-20 and EPD/RF-40 samples was measured by WST–8 assay based on the fraction of cell viability. Three different molar concentrations of extracts, namely 0.1, 0.2, 0.3, 0.5, 0.75 and 1 ml, were investigated. In this study, osteoblast-like MG-63 cells were used to determine the cell viability via an indirect method, and results are shown in Fig. 10.

Cell proliferation was evident for all samples and for all concentrations. The cell viability on EPD/RF-40 samples increased at all concentrations. However, in case of Ag-EPD and EPD/RF-20 samples, a dose-dependent cell proliferation was observed. Initially, cell viability decreased until 0.3 mL of extract, and then a minor increase in cell viability was observed, which concluded at a constant viability at higher molar contractions. Overall, Ag-EPD samples showed relative less viability when compared with EPD/RF-40 samples. According to the ICP ion release study, the release of silver ions from EPD coatings was three times greater as compared to the release from EPD/RF coatings, and this behavior can explain the cell viability results. Our aim was to obtain biocompatible and antibacterial coatings. It is apparent that, compared with pure Ag-EPD coatings, the multilayered EPD/RF coatings resulted in lower cytotoxicity at all concentrations. The multi-structured composite coatings (EPD/RF coatings) exhibited a sustained release of silver ions which reduced the potential cytotoxic effects of silver and increased cell viability in comparison to Ag-EPD coatings.

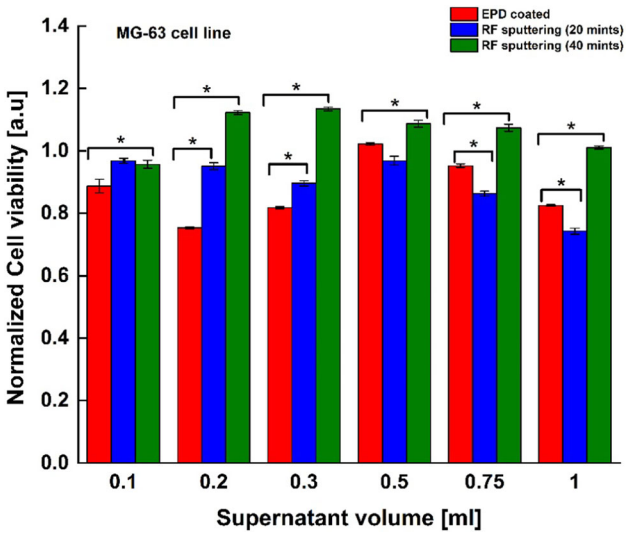

Figure 10 Cytotoxicity of MG-63 cell line after 2 days incubation calculated using WST-8 assay, polystyrene (PS), tissue culture plate was used as a control, and cell viability was normalised against the control. The (*) shows that the difference is statistically significant at $p < 0.05$ (Data represent the mean ± standard deviation of 5 samples).

The cell morphology, including cell–cell and cell-surface interactions was observed by SEM. Ag-EPD samples were toxic to MG-63 cells when cells were seeded directly on the surface of the coatings. SEM images of seeded MG-63 cells on the surface of EPD/RF-20 and EPD/RF-40 samples are shown in Fig. 11. The cells are well spread indicating a strong cell–cell and cell-surface adhesion. A typical phenotype expression of osteoblast-like cells was observed [17]. The qualitative analysis by SEM shows a substantial increase in cell density in EPD/RF-40 coatings in comparison to EPD/RF-20. The antibacterial results (see next section) are in accordance with the expected order of increasing antibacterial affect; i.e. Ag-EPD > EPD/RF-40 > EPD/RF-20. Taken together, the release of silver ions in multi-structured coatings (EPD/RF-coatings) leads to antibacterial effects without imparting negative results on the attachment and proliferation of osteoblast-like cells.

Antibacterial studies

Figure 12 shows the antibacterial potential of Ag-EPD, EPD/RF-20 and EPD/RF-40 coatings via a direct contact method. *E. coli and S. carnosus* were spread over the agar plates. The coatings were placed directly over the bacteria containing agar plates, and EPD coatings (PEEK/BG/MBGNs) were used as control sample. It was observed that the control sample did not exert any antibacterial effect. However, Ag-EPD, EPD/RF-20 and EPD/RF-40 coatings showed antibacterial potential against both *E. coli and S. carnosus* and formed an inhibition halo. Table 1 shows the size of inhibition zones, which was quantified using 'ImageJ'. Ag-EPD coatings show a maximum inhibition halo (1.261 cm^2) while in case of RF co-sputtered coatings, the diameter of the inhibition halo is directly proportional to the sputtering time. Higher sputtering times yielded relatively higher coating thickness and consequently higher total silver content in the top layer. Our results are in agreement with the previous findings [28], which concluded that silver nanocluster-silica composite coatings exhibited higher antibacterial effect by

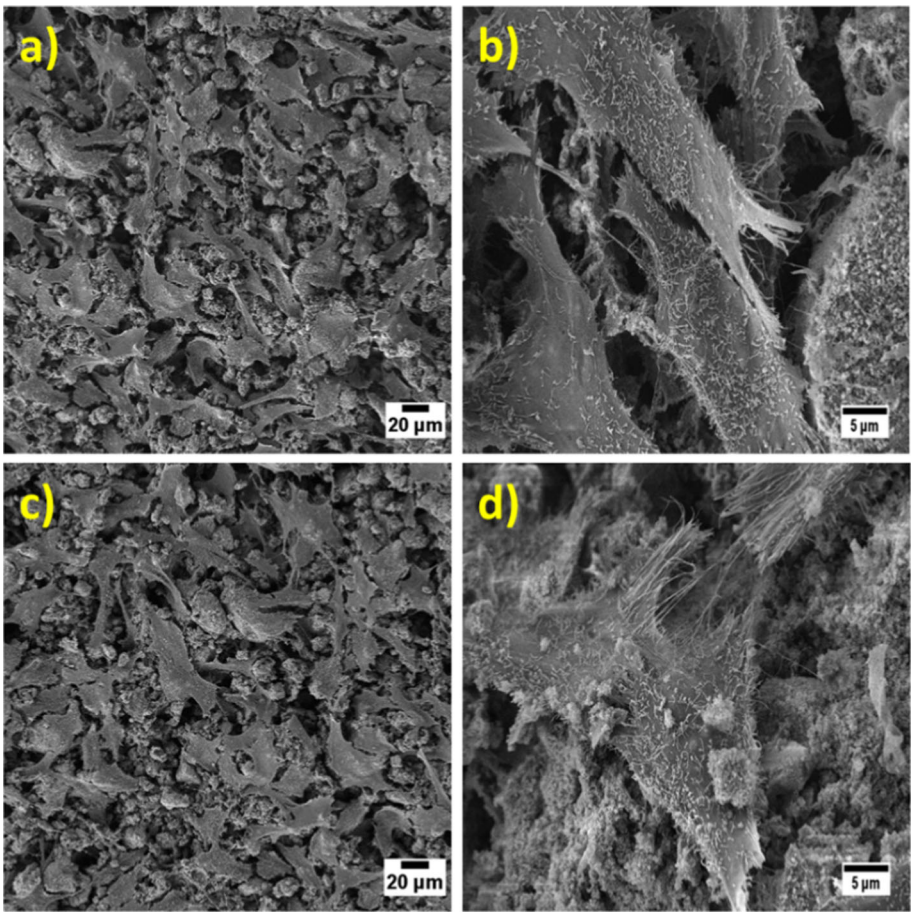

Figure 11 SEM images of cell spreading on EPD/RF-20 (**a** and **c**) and EPD/RF-40 (**b** and **d**) coatings after 2 days incubation in DMEM at low and high magnification.

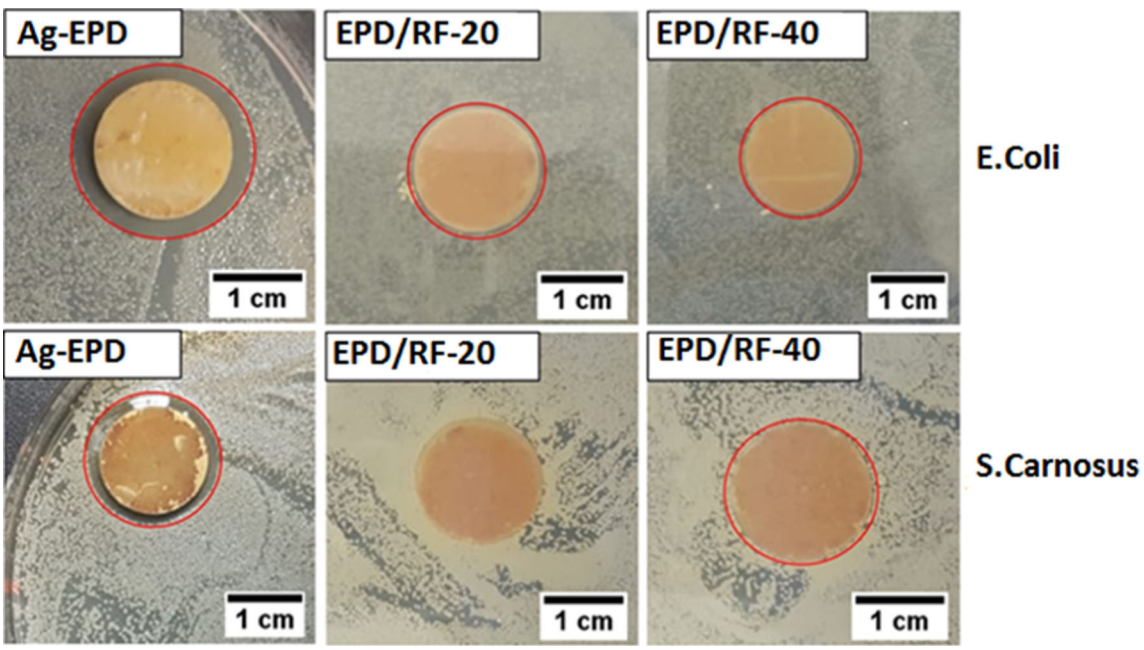

Figure 12 Typical results of inhibition halo tests against bacterial strains, when tested for 24 h.

Table 1 Results of inhibition halo test showing the area of inhibition for Ag-EPD, EPD/RF-20, and EPD/RF-40 coatings against *S. carnosus* and *E. coli*, when tested for 24 h

Sample name	*E. coli* (−)	*S. carnosus* (+)
EPD/RF-20	0.197 cm^2	0
EPD/RF-40	0.300 cm^2	0.239 cm^2
Ag-EPD	1.261 cm^2	0.848 cm^2
EPD	0	0

increasing the Ag/Si ratio [28]. It was noticed that EPD/RF-20 coatings did not show pronounced antibacterial effect against *S. carnosus*.

In the present coating design, stratified multi-structured EPD/RF-20 and EPD/RF-40 coatings showed a slow release of silver ions, which is a beneficial feature to reduce possible cytotoxic effects [26, 28]. Furthermore, the roughness and porosity of the bottom EPD layer contributes to the controlled and sustained release of silver ions. The antibacterial effects of silver nanoclusters is likely related to the release of silver ions (Ag +) in physiological conditions [43, 46, 47]. Silver ions are highly reactive towards electron donor species, such as respiratory enzymes or nucleic acids of bacteria, that can cause bacteria death [43, 47]. Silver ions exhibit a strong binding potential with DNA and proteins of bacteria. These binding interactions may favour the penetration of silver ions into the bacteria, which can result in the disruption of its DNA replication activity [48–50].

The combination of EPD and RF sputtering has thus led to biocompatiable and antibacterial coatings. Ag containing coatings deposited via EPD led to cytotoxic effects when tested with MG-63 cells. In contrast to this, when Ag was embedded in the silica matrix and deposited via RF sputtering controlled release of Ag ions was achieved resulting in desired antibacterial effect and biocompatibility. Furthermore, the composite bottom layer (PEEK/BG/MBGNs) could be deposited via EPD to achieve relatively high coating thickness and uniform co-deposition of the coating components [24].

Conclusion

In this study, we compared the silver release profile, antibacterial activity, adhesion strength and biocompatibility of PEEK/BG/Ag-MBGNs coatings (deposited via EPD) with multi-structured stratified coatings obtained via combination of RF co-sputtering and EPD (samples EPD/RF-20 and EPD/RF-40). The multi-structured coatings showed slower release of silver ions in comparison to the Ag-EPD layer. This controlled release of silver ions resulted in better cell viability (determined by the WST-8 assay with osteoblast-like MG-63 cells) in comparison to the Ag-EPD sample. Despite the slow release of silver ions from the EPD/RF-20 and EPD/RF-40 coatings, they showed strong antibacterial effect against Gram-positive and Gram-negative bacteria. Furthermore, EPD/RF-40 coatings developed HA crystals upon immersion in SBF, which indicates a bioactive character and potential bonding to bone. It can be concluded that the EPD/RF-20 and EPD/RF-40 coatings are suitable for further in-vivo investigations and eventually translation to clinical applications.

Acknowledgements

QN would like to thank the KMM-VIN Research Fellowship programme (http://www.kmm-vin.eu/fellowships) for providing a fellowship to carry out this research in collaboration with the Department of Applied Science and Technology, Politecnico di Torino, Italy.

Funding

Open Access funding enabled and organized by Projekt DEAL.

Compliance with ethical standards

Conflict of interest The authors declare that they have no conflict of interest.

Supplementary Information: The online version contains supplementary material available at https://doi.org/10.1007/s10853-020-05725-w.

References

[1] Park J, Lakes RS (2007) Biomaterials: an introduction, 3rd edn. Springer, Berlin

[2] Bronzino JD, Park JB (2002) Biomaterials: principles and applications. CRC Press, Boca Raton

[3] Ratner BD, Hoffman AS, Schoen FJ, Lemons JE (2004) Biomaterials science: an introduction to materials in medicine. Elsevier, New York

[4] Dee KC, D. a Puleo, R. Bizios, C.J. Wiley, (2002) Tissue-Biomaterial Interactions An Introduction To Tissue-Biomaterial Interactions. Springer, Berlin

[5] Heimann RB, Vu TA, Wayman ML (1997) Bioceramic coatings: State-of-the-art and recent development trends. Eur. J. Mineral 6:145–149

[6] Narayanan R, Seshadri SK, Kwon TY, Kim KH (2008) Calcium phosphate-based coatings on titanium and its alloys, J Biomed Mater Res. Part B Appl Biomater An Off J Soc Biomater Japanese Soc Biomater Aust Soc Biomater Korean Soc Biomater 85:279–299

[7] Nouri A, Wen C (2016) Introduction to surface coating and modification for metallic biomaterials, in: Surf. Coat. Modif. Met. Biomater., Elsevier. pp. 3–60

[8] Atiq M, Rehman U, Bastan FE, Nawaz Q, Goldmann WH, Maqbool M, Virtanen S, Boccaccini AR (2018) Electrophoretic deposition of lawsone loaded bioactive glass (BG)/chitosan composite on polyetheretherketone (PEEK)/BG layers as antibacterial and bioactive coating. J Biomed Mater Res Part A 2:1–12

[9] Atiq M, Rehman U, Azeem M, Schubert DW, Boccaccini AR, Rehman MAU, Munawar MA, Schubert DW, Boccaccini AR (2019) Electrophoretic deposition of chitosan/gelatin/bioactive glass composite coatings on 316L stainless steel: A design of experiment study. Surf Coatings Technol 358:976–986

[10] Hench LL (2006) The story of Bioglass®. J Mater Sci Mater Med 17:967–978

[11] Hench LL (2015) Opening paper 2015-some comments on bioglass: Four eras of discovery and development. Biomed Glas 1:1–11

[12] Nawaz Q, Rehman MAU, Burkovski A, Schmidt J, Beltrán AM, Shahid A, Alber NK, Peukert W, Boccaccini AR (2018) Synthesis and characterization of manganese containing mesoporous bioactive glass nanoparticles for biomedical applications. J Mater Sci Mater Med 5:64

[13] Zheng K, Boccaccini AR (2017) Sol-gel processing of bioactive glass nanoparticles: areview. Adv Colloid Interface Sci 249:363–373

[14] Zheng K, Dai X, Lu M, Huser N, Taccardi N, Boccaccini AR (2017) Synthesis of copper-containing bioactive glass nanoparticles using a modified Stober method for biomedical applications. Colloids Surfaces B Biointerfaces 150:159–167

[15] Kozon D, Zheng K, Boccardi E, Liu Y, Liverani L, Boccaccini AR (2016) Synthesis of monodispersed Ag-doped bioactive glass nanoparticles via surface modification. Materials (Basel) 9:225–232

[16] Zheng K, Wu J, Li W, Dippold D, Wan Y, Boccaccini AR (2018) Incorporation of Cu-containing bioactive glass nanoparticles in gelatin coated scaffolds enhances bioactivity and osteogenic activity. Am Chem Soc 4:1546–1557

[17] Nawaz Q, Rehman MAU, Roether JA, Yufei L, Grünewald A, Detsch R, Boccaccini AR (2019) Bioactive glass based scaffolds incorporating gelatin/manganese doped mesoporous bioactive glass nanoparticle coating. Ceram Int 45:14608–14613

[18] El-Rashidy AA, Waly G, Gad A, Hashem AA, Balasubramanian P, Kaya S, Boccaccini AR, Sami I (2018) Preparation and in vitro characterization of silver doped bioactive glass nanoparticles fabricated using a sol gel process and modified Stöber method. J Non Cryst Solids 483:26–36

[19] Baştan FEFEFE, Rehman MAU, Avcu YYYY, Avcu E, Üstel F, Boccaccini ARAR (2018) Electrophoretic co-deposition of PEEK-hydroxyapatite composite coatings for biomedical applications. Colloids Surfaces B Biointerfaces 169:176–182

[20] Rehman MAU, Bastan FE, Haider B, Boccaccini AR (2017) Electrophoretic deposition of PEEK/bioactive glass composite coatings for orthopedic implants: a design of experiments (DoE) study. Mater Des 130:223–230

[21] Avcu E, Baştan FE, Abdullah HZ, Ur Rehman MA, Yıldıran Avcu Y, Boccaccini AR (2019) Electrophoretic deposition of chitosan-based composite coatings for biomedical applications: a review. Prog Mater Sci 103:69–108

[22] Moskalewicz T, Zych A, Ukaszczyk A, Cholewa-Kowalska K, Kruk A, Dubiel B, Radziszewska A, Berent K, Gajewska M (2017) Electrophoretic deposition microstructure and corrosion resistance of porous Sol-Gel glass/

polyetheretherketone coatings on the Ti-13Nb-13Zr Alloy. Metall Mater Trans A Phys Metall Mater Sci 48:2660–2673

[23] Moskalewicz T, Seuss S, Boccaccini AR (2013) Microstructure and properties of composite polyetheretherketone/Bioglass® coatings deposited on Ti–6Al–7Nb alloy for medical applications. Appl Surf Sci 273:62–67

[24] Rehman MAU, Bastan FE, Nawaz A, Nawaz Q, Wadood A (2020) Electrophoretic deposition of PEEK/bioactive glass composite coatings on stainless steel for orthopedic applications: an optimization for in vitro bioactivity and adhesion strength. Int J Adv Manuf Technol 108:1849–1862

[25] Nawaz A, Bano S, Yasir M, Wadood A, Ur Rehman MA (2020) Ag and Mn-doped mesoporous bioactive glass nanoparticles incorporated into the chitosan/gelatin coatings deposited on PEEK/bioactive glass layers for favorable osteogenic differentiation and antibacterial activity. Mater Adv 1:1273–1284

[26] Seuss S, Heinloth M, Boccaccini AR (2015) Development of bioactive composite coatings based on combination of PEEK, bioactive glass and Ag nanoparticles with antibacterial properties. Surf Coatings Technol 301:100–105

[27] Rehman MAU, Chen Q, Braem A, Shaffer MSP, Boccaccini AR (2020) Electrophoretic deposition of carbon nanotubes: recent progress and remaining challenges. Int Mater Rev 5:1–30

[28] Rehman MAU, Ferraris S, Goldmann WH, Perero S, Bastan FE, Nawaz Q, Di Confiengo GG, Ferraris M, Boccaccini AR (2017) Antibacterial and bioactive coatings based on radio frequency co-sputtering of silver nanocluster-silica coatings on PEEK/Bioactive glass layers obtained by electrophoretic deposition. ACS Appl Mater Interfaces 9:32489–32497

[29] Safavi MS, Surmeneva MA, Surmenev RA, Khalil-Allafi J (2020) RF-magnetron sputter deposited hydroxyapatite-based composite & multilayer coatings: a systematic review from mechanical, corrosion, and biological points of view. Ceram Int. https://doi.org/10.1016/j.ceramint.2020.09.274

[30] Chernozem RV, Surmeneva MA, Krause B, Baumbach T, Ignatov VP, Tyurin AI, Loza K, Epple M, Surmenev RA (2017) Hybrid biocomposites based on titania nanotubes and a hydroxyapatite coating deposited by RF-magnetron sputtering: Surface topography, structure and mechanical properties. Appl Surf Sci 426:229–237

[31] Surmenev RA, Surmeneva MA, Grubova IY, Chernozem RV, Krause B, Baumbach T, Loza K, Epple M (2017) RF magnetron sputtering of a hydroxyapatite target: a comparison study on polytetrafluorethylene and titanium substrates. Appl Surf Sci 414:335–344

[32] Muzio G, Perero S, Miola M, Oraldi M, Ferraris S, Vern E, Festa F, Canuto RA (2016) Biocompatibility versus peritoneal mesothelial cells of polypropylene prostheses for hernia repair coated with a thin silica/silver layer. J Biomed Master Res B Appl Biomater 5:1–8

[33] Ferraris M, Perero S, Miola M, Ferraris S, Gautier G, Maina G, Fucale G, Verne E (2010) Chemical, mechanical, and antibacterial properties of silver nanocluster-silica composite coatings obtained by sputtering. Adv Eng Mater 12:276–282

[34] Ferraris M, Perero S, Miola M, Ferraris S, Verné E, Morgiel J (2010) Silver nanocluster–silica composite coatings with antibacterial properties. Mater Chem Phys 120:123–126

[35] Kokubo T, Takadama H (2006) How useful is SBF in predicting in vivo bone bioactivity? Biomaterials 27:2907–2915

[36] Sak A, Moskalewicz T, Zimowski S, Cieniek Ł, Dubiel B, Radziszewska A, Kot M, Łukaszczyk A (2016) Influence of polyetheretherketone coatings on the Ti-13Nb-13Zr titanium alloy's bio-tribological properties and corrosion resistance. Mater Sci Eng C 63:52–61

[37] Balagna C, Perero S, Ferraris S, Miola M, Fucale G, Manfredotti C, Battiato A, Santella D, Vernè E, Vittone E, Ferraris M (2012) Antibact coating on polymer for space application. Mater Chem Phys 135:714–722

[38] Balagna C, Irfan M, Perero S, Miola M, Maina G, Santella D, Simone A (2017) Characterization of antibacterial silver nanocluster/silica composite coating on high performance Kevlar® textile. Surf Coatings Technol 321:438–447

[39] Irfan M, Perero S, Miola M, Maina G, Ferri A, Ferraris M, Balagna C (2017) Antimicrobial functionalization of cotton fabric with silver nanoclusters/silica composite coating via RF co-sputtering technique. Cellulose 24:2331–2345

[40] Ferraris M, Perero S, Ferraris S, Miola M, Vernè E, Skoglund S, Blomberg E, Odnevall Wallinder I (2017) Antibacterial silver nanocluster/silica composite coatings on stainless steel. Appl Surf Sci 396:1546–1555

[41] Rehman MAU, Bastan FE, Nawaz Q, Boccaccini AR (2018) Electrophoretic deposition of lawsone loaded nanoscale silicate glass/chitosan composite on PEEK/BG layers. Electrochem Soc Tras 82:45–50

[42] Virk RS, Rehman MAU, Munawar MA, Schubert DW, Goldmann WH, Dusza J, Boccaccini AR (2019) Curcumin-containing orthopedic implant coatings deposited on polyether-ether-ketone/bioactive glass/hexagonal boron nitride layers by electrophoretic deposition. Coatings 9:572

[43] Pishbin F, Mouriño V, Gilchrist JB, McComb DW, Kreppel S, Salih V, Ryan MP, Boccaccini AR (2013) Single-step electrochemical deposition of antimicrobial orthopaedic coatings based on a bioactive glass/chitosan/nano-silver composite system. Acta Biomater 9:7469–7479

[44] Pishbin F, Mourino V, Flor S, Kreppel S, Salih V, Ryan MP, Boccaccini AR (2014) Electrophoretic deposition of gentamicin-loaded bioactive glass/chitosan composite coatings

for orthopaedic implants. ACS Appl Mater Interfaces 6:8796–8806

[45] Nawaz A, Ur Rehman MA (2018) Chitosan/gelatin-based bioactive and antibacterial coatings deposited via electrophoretic deposition. J Appl Polym Sci 50:220

[46] Saleem O, Wahaj M, Akhtar MA, Ur Rehman MA (2020) Fabrication and characterization of Ag-Sr-substituted hydroxyapatite/chitosan coatings deposited via electrophoretic deposition: a design of experiment study. ACS Omega 5:22984–22992

[47] Simchi A, Tamjid E, Pishbin F, Boccaccini AR (2011) Recent progress in inorganic and composite coatings with bactericidal capability for orthopaedic applications, nanomedicine Nanotechnology. Biol Med 7:22–39

[48] Ferraris M, Balagna C, Perero S, Miola M, Ferraris S, Baino F, Battiato A, Manfredotti C, Vittone E (2012) Silver nanocluster silica composite coatings obtained by sputtering for antibacterial applications. Conf Ser Mater Sci Eng 4:10–60

[49] Kawashita M, Tsuneyama S, Miyaji F, Kokubo T, Kozuka H, Yamamoto K (2000) Antibacterial silver-containing silica glass prepared by sol gel method. Biomaterials 21:393–398

[50] Kim T-S, Cha J-R, Gong M-S (2018) Investigation of the antimicrobial and wound healing properties of silver nanoparticle-loaded cotton prepared using silver carbamate. Text Res J 88:766–776